



Supplement of

Newly identified climatically and environmentally significant high-latitude dust sources

Outi Meinander et al.

Correspondence to: Outi Meinander (outi.meinander@fmi.fi)

The copyright of individual parts of the supplement might differ from the article licence.

1 **Supplementary Animation**
2 http://www.seevccc.rs/HLDpaper/NMMB_DREAM_circumpolar_dustload_animation.gif

3 **Supplementary Tables and Figures**

4
5 **Table S1. The contemporary category of the newly identified high-latitude dust sources included in this study based on the**
6 **currently available observations. The number refers to the source number of the map in Figure 1. Also, McMurdo Dry Valley is**
7 **estimated to best fit Category 3 and the McMurdo Ice Shelf ‘debris bands’ to Category 2.**
8

Cat	HLD No.	Description	Climatic or environmental significance	Criteria
1	30, 31, 32, 34	Active source	High	Frequently active dust source with >10 dust events documented
2	25, 26, 27, 35	Moderately active source	Moderate	5–10 dust events documented or a smaller potential source area
3	1, 2-24, 28-29, 33, 36 –64	Source with unknown activity	Small/Currently unknown	Infrequent activity or a new source with 1–5 dust events documented

9
10 **Table S2. Iceland dust sources and observations on dust events identified in this study based on satellite images of 2002–2011,**
11 **source numbers 23–35 in Figure 1.**
12

Location in Iceland	Satellite observations
---------------------	------------------------

No. 23 Reykjanes	2 events, 2004 and 2011
No. 24 Eyrabakki	3 events, 2002–2011
No. 25 Hagavatnssvæði	8 events, 2002–2011
No. 26 Fljótshlíð	8 events, 2002–2011
No. 27 Langisjór	5 events in 2010; 3 events in 2002–2011
No. 28 Eldhraun/Landbrot	3 events 2002–2011
No. 29 Eldhraun	3 events 2002–2011
No. 30 Klausturfjara	17 events 2002–2011
No. 31 Núpsvötn	39 events 2002–2011
No. 32 Holuhraun	29 events 2002–2011
No. 33 Vikurhraun/Vikursandur	2 events 2002–2011
No. 34 Höfn í Hornarfirði	13 events 2002–2011
No. 35 Lónsvík	8 events 2002–2011

13

14 **Table S3. West coast of Greenland observations for the new dust sources identified for the first time in this study (No. 53–58 in**
15 **Fig. 1), based on satellite observations from 2021 and earlier satellite observations for sources identified in East Greenland and**
16 **Canada (No. 59–64), north of 70°N**

17

Latitude	Longitude	No.	Description	Dust example	Observed events
63.5059	-51.0454	53	West coast of Greenland, the source appears to be in the delta area, not in the valley	https://go.nasa.gov/3biOSt9	26 Oct 2021
62.2421	-49.0481	54	West coast of Greenland, the source appears to be a	https://go.nasa.gov/3Gw80SV	23/25 Oct 2021

			small valley with a glacier		
63.5163	-50.9652	55	West coast of Greenland, source appears to be the delta area (Sentinel shows dust plumes up 10 km from the coast, east of delta)	https://go.nasa.gov/3Ct5cmY	18,19,25,26 Oct 2021
65.7621	-51.2866	56	West coast of Greenland, a very narrow valley (not clear if dust comes from the valley or termination tip of glacier). Clear dust plumes when flipping images Aqua/Terra	https://go.nasa.gov/2ZBLvv2	18 and 22 Oct 2021
62.4791	-50.2146	57	West coast of Greenland, small trip of land between sea and glacier	https://go.nasa.gov/2ZyWbca	18 Oct 2021
67.359	-52.3693	58	West coast of Greenland, a short valley, several dust clouds appear	https://go.nasa.gov/3vU4qwR	18 Oct 2021
71.8288	-22.8017	59	East Greenland	https://go.nasa.gov/3pOPjng	3 Oct 2019
70.4565	-22.2694	60	East Greenland	https://go.nasa.gov/3Gx1paM	15 Sep 2020
78.0407	-21.4572	61	East Greenland	https://go.nasa.gov/3Gw4g3R	24 Sep 2003
81.3073	-78.2145	62	Canada	https://go.nasa.gov/3mxJxEZ	2 July 2020
71.8426	-22.7902	63	East Greenland, better seen in S2 and L8	https://go.nasa.gov/3Bt9jy2	30 Sept 2018
72.3906	-25.1555	64	East Greenland	https://go.nasa.gov/3vXOWb6	23 Sep 2003

Table S4. Locations of the HLD sources (no. 1-64 in Fig. 1) and G-SDS-SBM source intensity (SI) values at location; maximum values found in certain environments given location (areas within the distance from location of 30 arcsec, 0.1°, 0.5°, and 1°); SI is undefined (-99.0) if location mark is not over land; area south of 60°S is not included in G-SDS-SBM, and values at locations in this area are marked with a dash.

No.	lat	lon	at loc.		30 arcsec		0.1°		0.5°		1°	
			max	min	max	min	max	min	max	min	max	min
1	57.6482	10.4059	0.8	0.0	0.9	0.0	1.0	0.0	1.0	1.0	1.0	1.0
2	63.2	75.5	0.1	0.0	0.1	0.0	0.1	0.0	0.3	0.2	0.5	0.2

3	60.1	71.4	0.0	0.0	0.0	0.0	0.3	0.0	0.3	0.0	0.8	0.3
4	58.9	69.2	0.0	0.0	0.0	0.0	0.2	0.0	0.7	0.3	0.8	0.3
5	56.5	67.5	0.1	0.0	0.2	0.0	0.2	0.0	0.3	0.1	0.5	0.1
6	67.6	33.4	0.0	0.0	0.0	0.0	0.8	0.0	0.9	0.0	1.0	0.0
7	51.3	88.5	0.0	0.0	0.0	0.0	0.2	0.0	0.4	0.0	0.4	0.2
8	47.3	66.7	0.5	0.0	0.5	0.0	0.6	0.3	0.7	0.4	1.0	0.7
9	-77.9	165.2	-	-	-	-	-	-	-	-	-	-
10	63.5	-18.2	1.0	0.0	1.0	0.0	1.0	1.0	1.0	1.0	1.0	1.0
11	71.4	128.5	0.0	0.0	0.3	0.0	0.4	0.0	1.0	0.0	1.0	0.0
12	81.7	-71.1	0.7	0.0	0.8	0.0	1.0	0.0	1.0	0.0	1.0	0.0
13	77	16	-99.0	-99.0	-99.0	-99.0	0.9	0.0	1.0	0.0	1.0	0.0
14	60.5	-144.9	0.6	0.0	0.9	0.0	1.0	0.0	1.0	0.5	1.0	0.5
15	56.0054	8.1138	0.0	0.0	0.9	0.0	1.0	0.0	1.0	1.0	1.0	1.0
16	69.36	-123.97	0.7	0.0	1.0	0.0	1.0	0.0	1.0	0.0	1.0	0.0
17	-45.48	-68.78	0.0	0.0	0.7	0.7	0.8	0.7	0.9	0.8	0.9	0.8
18	77	15	-99.0	-99.0	-99.0	-99.0	1.0	0.0	1.0	0.0	1.0	0.0
19	-63.9	-57.9	-	-	-	-	-	-	-	-	-	-
20	-64.2	-56.6	-	-	-	-	-	-	-	-	-	-
21	70.4	-52.5	0.5	0.0	0.6	0.0	0.8	0.0	1.0	0.0	1.0	0.0
22	78.7	15.7	0.3	0.0	0.3	0.0	0.7	0.0	1.0	0.0	1.0	0.0
23	63.85	- 22.2163 5	0.0	0.0	0.7	0.1	1.0	0.9	1.0	1.0	1.0	1.0
24	63.87	- 21.1888 5	0.0	0.0	1.0	0.0	1.0	0.0	1.0	1.0	1.0	1.0
25	64.47	- 20.3270 2	0.4	0.0	0.4	0.0	0.6	0.2	0.8	0.5	1.0	1.0
26	63.72	- 20.1401 3	0.2	0.0	0.2	0.0	0.3	0.1	1.0	1.0	1.0	1.0
27	64.14	- 18.2902 2	0.3	0.0	0.3	0.0	0.4	0.0	0.9	0.7	1.0	1.0
28	63.69	- 18.2001 2	0.0	0.0	0.4	0.0	1.0	1.0	1.0	1.0	1.0	1.0
29	64.03	- 17.9927 6	0.0	0.0	0.2	0.0	0.3	0.0	1.0	1.0	1.0	1.0

30	63.7	- 17.7592 5	0.9	0.0	0.9	0.0	1.0	0.7	1.0	1.0	1.0	1.0
31	63.91	- 17.5464 0	0.6	0.0	0.6	0.5	1.0	0.5	1.0	1.0	1.0	1.0
32	64.84	- 16.8455 0	0.2	0.0	0.3	0.0	0.5	0.0	0.5	0.0	1.0	1.0
33	65.02	- 16.4949 2	0.0	0.0	0.2	0.0	0.5	0.0	0.6	0.3	1.0	1.0
34	64.24	- 15.2144 3	0.0	0.0	0.0	0.0	1.0	0.1	1.0	1.0	1.0	1.0
35	64.38	- 14.7674 3	0.3	0.0	0.7	0.0	1.0	1.0	1.0	1.0	1.0	1.0
36	-45.56	-68.7378	0.0	0.0	0.7	0.6	0.8	0.7	0.9	0.8	0.9	0.9
37	-53.217	-68.6934	0.0	0.0	0.3	0.2	1.0	0.9	1.0	1.0	1.0	1.0
38	-53.78	-67.8064	0.9	0.0	1.0	0.0	1.0	0.9	1.0	1.0	1.0	1.0
39	-49.53	-68.1744	0.9	0.9	0.9	0.9	1.0	1.0	1.0	1.0	1.0	1.0
40	-47.61	-65.7979	1.0	1.0	1.0	1.0	1.0	1.0	1.0	1.0	1.0	1.0
41	-47.94	-66.2073	0.8	0.7	0.8	0.7	1.0	1.0	1.0	1.0	1.0	1.0
42	-46.72	-69.0699	0.8	0.7	0.8	0.7	0.9	0.8	0.9	0.8	0.9	0.9
43	-46.53	-69.401	0.7	0.7	0.7	0.7	0.7	0.7	0.9	0.9	0.9	0.9
44	-48.54	-67.015	0.8	0.8	0.8	0.8	1.0	1.0	1.0	1.0	1.0	1.0
45	-41.14	-69.46	0.0	0.0	0.5	0.3	0.6	0.4	0.6	0.5	0.8	0.5
46	70.47	-52.88	0.5	0.0	0.9	0.0	0.9	0.0	1.0	0.0	1.0	0.0
47	71.36	-24.53	0.6	0.0	0.6	0.0	1.0	0.0	1.0	0.0	1.0	0.0
48	47.6	-111.25	0.5	0.1	0.8	0.1	0.8	0.7	1.0	0.7	1.0	0.9
49	67.87	44.13	1.0	0.0	1.0	0.0	1.0	0.0	1.0	0.0	1.0	0.0
50	60.9987	- 138.529 4	0.6	0.0	0.7	0.3	0.7	0.3	0.9	0.5	1.0	0.6
51	56.4772	12.9260	0.0	0.0	0.0	0.0	0.9	0.0	1.0	0.6	1.0	0.6
52	70.7583	- 11.6444	-	-	-	-	-	-	-	-	-	-
53	63.5059	-51.0454	0.0	0.0	0.5	0.0	1.0	0.2	1.0	1.0	1.0	1.0
54	62.2421	-49.0481	0.4	0.0	0.5	0.0	0.8	0.3	1.0	1.0	1.0	1.0
55	63.5163	-50.9652	0.0	0.0	0.5	0.0	1.0	0.2	1.0	1.0	1.0	1.0

56	65.7621	-51.2866	0.0	0.0	0.6	0.0	0.9	0.0	0.9	0.0	1.0	1.0
57	62.4791	-50.2146	0.5	0.0	0.6	0.0	0.6	0.3	1.0	0.9	1.0	1.0
58	67.359	-52.3693	0.4	0.0	0.5	0.0	1.0	0.0	1.0	0.1	1.0	1.0
59	71.8288	-22.8017	0.0	0.0	1.0	0.0	1.0	0.0	1.0	0.0	1.0	0.0
60	70.4565	-22.2694	0.9	0.0	1.0	0.0	1.0	0.0	1.0	0.0	1.0	0.0
61	78.0407	-21.4572	1.0	0.0	1.0	0.0	1.0	0.0	1.0	0.0	1.0	0.0
62	81.3073	-78.2145	0.0	0.0	0.0	0.0	0.0	0.0	0.9	0.0	1.0	0.0
63	71.8426	-22.7902	0.0	0.0	0.0	0.0	1.0	0.0	1.0	0.0	1.0	0.0
64	72.3906	-25.1555	-99.0	-99.0	-99.0	-99.0	0.3	0.0	0.4	0.0	1.0	0.0

24
25
26

27
28
29
30

Table S5. Number of locations for north and south HLD regions that have SI values above a certain threshold (0.9, 0.8, 0.7, 0.6, 0.5, 0.4), depending on the environment size (30 arcsec, 0.1°, 0.5°, and 1°)

No.	lat	lon	at loc.		30 arcsec		0.1°		0.5°		1°	
			max	min	max	min	max	min	max	min	max	min
NORTH HLD REGION (NORTH OF 50°N)												
SI ≥ 0.9			5	0	12	0	27	4	39	16	44	23
SI ≥ 0.8			6	0	14	0	31	4	40	16	46	23
SI ≥ 0.7			8	0	17	0	33	6	42	18	46	24
SI ≥ 0.6			12	0	22	0	36	6	43	19	46	26
SI ≥ 0.5			17	0	27	1	38	7	44	22	48	27
SI ≥ 0.4			20	0	29	1	40	7	46	23	49	27
SOUTH HLD REGION (SOUTH OF 40°S)												
SI ≥ 0.9			3	2	3	2	7	6	10	7	10	9
SI ≥ 0.8			6	3	6	3	9	7	10	10	11	10
SI ≥ 0.7			7	6	9	7	10	10	10	10	11	10
SI ≥ 0.6			7	6	9	8	11	10	11	10	11	10
SI ≥ 0.5			7	6	10	8	11	10	11	11	11	11
SI ≥ 0.4			7	6	10	8	11	11	11	11	11	11

31
32
33
34

Table S6. Mineralogical and elemental composition of PM2 and PM1000 of soils in Western Siberia.

Proxy	HLD no.2 (Podzols)			HLD no.3 (Retisols and Gleysols)				HLD no.4 (Retisols and Gleysols)				HLD no.5 (Phaeozems and Stagnosols)			
	PM2, n=1		PM1000, n=10	PM2, n=4		PM1000, n=7		PM2, n=5		PM1000, n=5		PM2, n=8		PM1000, n=11	
	M	M	σ	M	σ	M	σ	M	σ	M	σ	M	σ	M	σ
Smectite, %	36.7	0.0	0.0	51.5	4.1	13.7	10.4	46.8	5.5	17.7	10.5	47.6	11.6	23.2	8.7
Illite, %	5.5	2.9	1.0	8.7	1.4	9.3	0.8	8.1	0.9	6.3	0.7	8.3	2.2	10.1	1.5
I/Sm, %	23.6	<0.1	-	18.2	1.0	<0.1	-	20.1	5.1	<0.1	-	26.0	10.1	<0.1	-
Kaolinite, %	6.7	1.4	1.2	3.5	0.8	2.3	0.6	6.5	2.5	2.2	1.1	5.3	1.7	3.4	0.7
Chlorite, %	2.1	0.4	0.5	2.4	0.8	1.0	0.7	1.1	1.1	2.1	0.8	1.9	0.5	1.7	0.7
Pls, %	6.4	5.5	2.7	4.3	0.8	15.5	3.2	4.5	0.7	14.6	3.4	3.5	1.3	13.8	2.5
PFS, %	7.1	4.9	3.0	4.9	1.3	8.3	1.9	4.3	0.9	8.3	1.4	5.4	1.8	8.1	1.6
Quartz, %	11.2	84.6	6.8	5.7	1.7	49.8	10.2	7.6	4.5	48.7	8.9	4.1	2.6	38.4	6.2
Calcite, %	0.8	0.4	0.2	1.1	0.2	0.0	0.0	1.0	0.7	0.0	0.0	2.0	2.6	1.4	3.1
TOC, %	n.a.	1.7	3.7	1.0	1.0	4.7	7.3	6.0	4.3	1.8	2.9	2.4	3.1	1.0	1.4
Na ₂ O, %	0.71	0.54	0.32	0.25	0.14	0.99	0.33	0.19	0.09	1.23	0.26	0.18	0.05	0.87	0.24
MgO, %	1.14	0.13	0.11	1.97	0.22	1.18	0.67	1.73	0.37	1.28	0.29	2.33	0.29	1.75	0.43
Al ₂ O ₃ , %	20.7	3.5	2.0	15.6	3.1	10.9	2.8	16.2	2.7	10.9	1.3	17.2	3.3	12.0	1.9
P ₂ O ₅ , %	0.34	0.47	0.47	0.34	0.47	0.13	0.07	0.44	0.26	0.16	0.15	0.25	0.21	0.27	0.41
S, %	0.24	0.04	0.02	0.14	0.25	0.09	0.04	0.12	0.15	<0.1	-	0.06	0.07	0.06	0.02
K ₂ O, %	1.64	1.18	0.54	1.86	0.32	1.74	0.29	1.59	0.17	1.88	0.16	2.50	0.42	2.14	0.26
CaO, %	0.48	0.16	0.07	1.20	0.34	0.75	0.36	1.05	0.47	1.18	0.36	2.32	1.77	1.97	2.00

TiO ₂ , %	0.92	0.33	0.19	0.71	0.14	1.03	0.04	0.61	0.14	1.00	0.21	0.62	0.11	0.97	0.08
MnO, %	0.29	0.02	0.01	0.10	0.06	0.06	0.04	0.13	0.08	0.10	0.09	0.07	0.04	0.12	0.08
Fe ₂ O ₃ , %	9.1	0.5	0.4	8.8	2.2	3.6	2.0	9.2	2.8	4.9	1.2	8.8	1.1	5.3	1.5
V, mg/kg	171	30	17	174	45	123	24	164	35	115	14	168	24	140	16
Cr, mg/kg	754	36	26	298	251	129	20	231	67	144	16	216	96	154	28
Co, mg/kg	62	<10	-	22	4.4	15.3	3.5	26.2	6.4	20	7.5	17	2.1	17	3.8
Ni, mg/kg	182	<10	-	115	45	29	15	85	8.0	32	9.4	90	25	47	11
Cu, mg/kg	59	<10	-	54	5.0	20	5.3	38	10	15	1.5	48	9.9	28	4.5
Zn, mg/kg	180	26	8.1	144	21	50	22	136	25	61	17	126	9.7	75	12
As, mg/kg	15	<10	-	13	2,4	<10	-	14	4.5	<10	-	12	3.2	<10	-
Pb, mg/kg	36	<10	-	32	21	19	5.3	28	7.1	23.3	12	19	3.3	27	5.1

37 I/Sm – illite-smectite mixed-layer minerals with predomination of illite interlayers, PLs – Plagioclases PFS – potassium
38 feldspars, TOC – total organic carbon

39

Table S7. Some characteristics of tailing ponds on the Kola Peninsula (Masloboev et al., 2016).

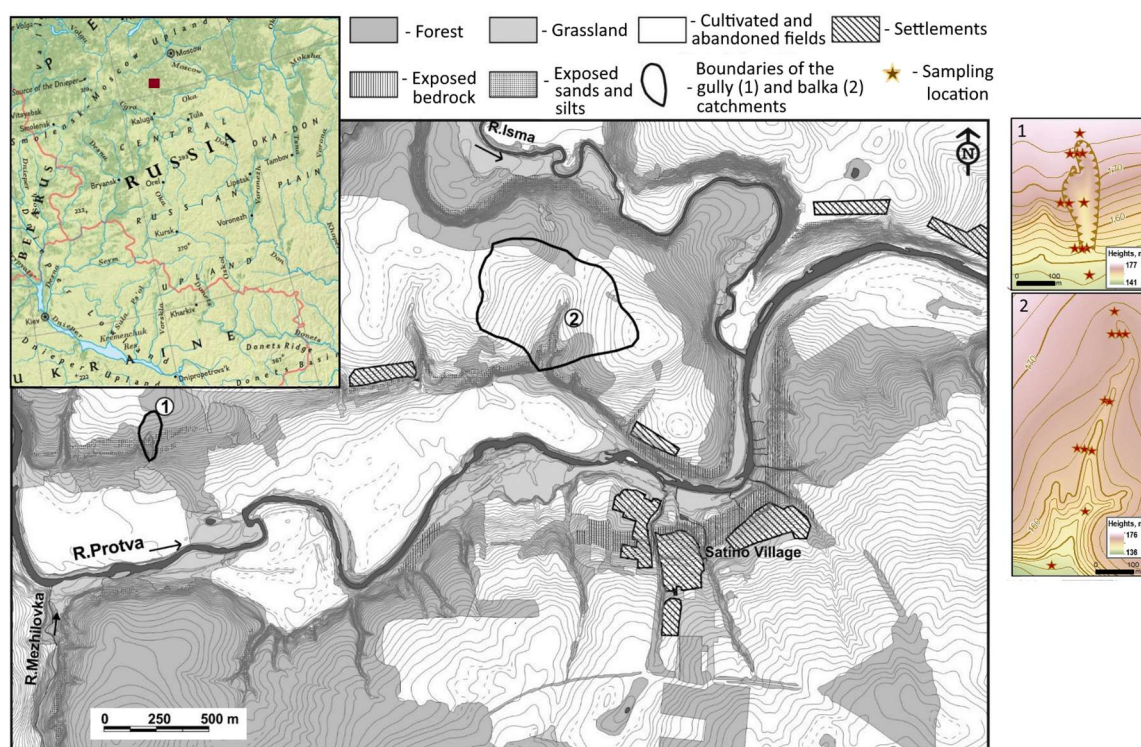
No.	Object	Exploitation period	Total area, ha	Resource, mln. t
1	Tailing pond of processing plant no. 1 of the Pechenganickel works, JSC Kola MMC	1945–1994	1033	~220
2	Tailing pond of processing plant no. 2 of the Pechenganickel works, JSC Kola MMC	1965–present time		22.4
3	Tailing pond of processing plant of the Severonikel works, JSC Kola MMC	1935–1978	No data	5.3
4	Dumps of granulated slag of the Pechenganickel works, JSC Kola MMC	1945–present time	80	47
5	Tailing pond no. 1 and no. 2 of crushing and processing plant, JSC Olkon	1954–present time	1400	~300
6	Tailing pond of apatite-nepheline processing plant no.1 (ANOF-1), JSC Apatit	1957–1963	120	24.4
7	Tailing pond of apatite-nepheline processing plant no. 2 (ANOF-2), JSC Apatit	1963–present time	1652	~550
8	Tailing pond of apatite-nepheline processing plant no. 3 (ANOF-3), JSC Apatit	1988–present time	1158	~250
9	Tailing pond of JSC Kovdorskiy GOK, (field no. 1)	1962–1980	330	53.8
10	Tailing pond of JSC Kovdorskiy GOK, (field no. 2)	1988–present time	900	80
11	Tailing pond of LLC Lovoserskiy GOK	1951–present time	No data	12
12	Tailing pond of LLC Kovdorslyuda	1959 – present	35	6

Topsoil (0–10 cm) samples were collected along several transects (Samonova and Aseyeva, 2020), crossing two small erosional landforms—a gully and a balka (Fig 1A). The collected bulk samples (n=22) were physically fractionated into five particle-sized fractions (250–1000, 50–250, 10–50, 1–10, and <1 μm , n=100). The boundaries among particle size classes were defined according to the Russian conventional fraction groups: coarse and medium sand (250–1000 μm), fine sand (50–250 μm), coarse silt (10–50 μm), medium and fine silt (1–10 μm), and clay (<1 μm). The concentrations of Al, Fe, Mn, Ti, Li, Be, Sc, V, Cr, Co, Ni, Cu, Zn, Ga, As, Rb, Mo, Cd, Sn, Sb, Cs, Pb, Ta, Tl, Bi, Th, Y, Nb, Ba, U, Zr, Sr, and Hf were determined on Elan-6100 and Optima-4300 DV spectrometers (Perkin Elmer Inc., USA) by ICP-AES/MS after the samples were digested in a mixture of acids (NSAM-499-AES/MS method). In physical fractionation, the sand fractions were separated from the bulk soil samples by wet sieving, while the silt and clay fractions were obtained by sedimentation and siphoning during times determined by Stokes' law.

The measured concentrations and element distribution among soil particle-sized fractions are shown in Figs. 2A, 3A, and 4A. Because of the different ways in which the elements can occur in the soils (Samonova and Aseyeva, 2020), their distribution among particle-sized fractions varies. However, some common patterns in partitioning the elements exist, which allowed us to combine them into several distinct groups (groups A, B, and C). According to our results, most of the elements (Al, Cd, Zn, Sc, V, Tl, Pb, Rb, Ti, Nb, Th, Y, U, Li, Cs, Be, and Ga) showed the progressive accumulation from the coarser to the finer fractions and a maximum of the element concentration in the clay fraction (Fig.2A). The predominant accumulation of metals in the fine fractions was reported earlier for the natural and polluted soils (Hardy and Cornu, 2006; Ljung et al., 2006), suggesting these elements are mainly found in the secondary minerals such as phyllosilicate clays, where they occur as structural components or adsorbed ions. A more detailed study of the element partitioning showed that group A was not homogeneous because of some differences in the distribution of the elements between the two sand fractions, which allowed us to identify several subgroups of the elements. The first subgroup (Al, Cd, Zn, Sc, V, Tl, Pb, and Rb) included the elements partitioned equally between the two sand fractions. The second contained Ti, Nb, Th, Y, and U, with higher affinity to the finer sand fraction, presumably due to the preferential accumulation of stable minerals like rutile and titanite in the fine sand and silt fractions. The third included the lithophile elements (Li, Cs, Be, Ga) associated more closely with the coarser sand fraction than the fine sand fraction.

Unlike group A, the elements from group B had minimal concentrations, not in the sand but the silt fractions, specifically the coarse silt fraction (Cr, Ni, Sn, Bi, Sb, As, Mn, and Co) or both silt fractions (Fe and Mo). However, the major element hosting a particle-sized fraction remained the same (the clay fraction). Most of the elements comprising this group participate in redox reactions and belong to the arsenic group or represent typical elements of the ferro-family. The latter group can occur in soils as structural components of primary ferrous minerals or/and as co-precipitates in secondary Fe-Mn (hydr)oxides. Most of the elements from group B did not concentrate in the sand fractions, except for Mn, Co, and Mo, which, in some cases, displayed

76 two concentration maxima (one in clay and one in sand). Such bimodal distribution was reported earlier and can be explained
 77 by the presence of several hosting minerals and phases having high retention for these metals. In the clay, Mn and Co are
 78 associated with secondary clay minerals. However, in the sand, they seem bound to newly formed Mn (hydr)oxides.
 79 The last group (group C) incorporated stable elements Zr and Hf. Their maximum concentrations were observed in the silt
 80 fractions, with a maximum in the coarse silt and a minimum in the coarse and medium sand fractions. Such distribution among
 81 different particle-sized fractions can be explained by the occurrence of these elements in detrital grains of primary accessory
 82 minerals, such as zircon, usually concentrated in the fine sand to coarse silt fractions.
 83 In conclusion, our geochemical study conducted in the central part of European Russia showed that most of the elements in
 84 the upper horizons of typical silty soils displayed progressive accumulation in the finer fractions. However, our data also
 85 proves that the preferential association of the elements with particle-sized fractions is not limited to the clay fraction. Metals
 86 such as Mn and Co tend to have bimodal distribution with concentration maxima in the clay and sand fractions. The partitioning
 87 of Zr, Hf, Nb, Ti, U, and Y accumulating in the silt fractions is governed by their presence in the mineral structure of accessory
 88 minerals that are stable during transport, physicochemical weathering, and soil formation. In many cases, the coarse silt
 89 fraction, with particle sizes of 10–50 μm , is depleted in elements, which can stem from its loessial origin.



93 **Figure S1. Map of the study area in Central European Russia with the study objects and sampling locations (Samonova and Aseyeva,**
94 **2020).**
95
96

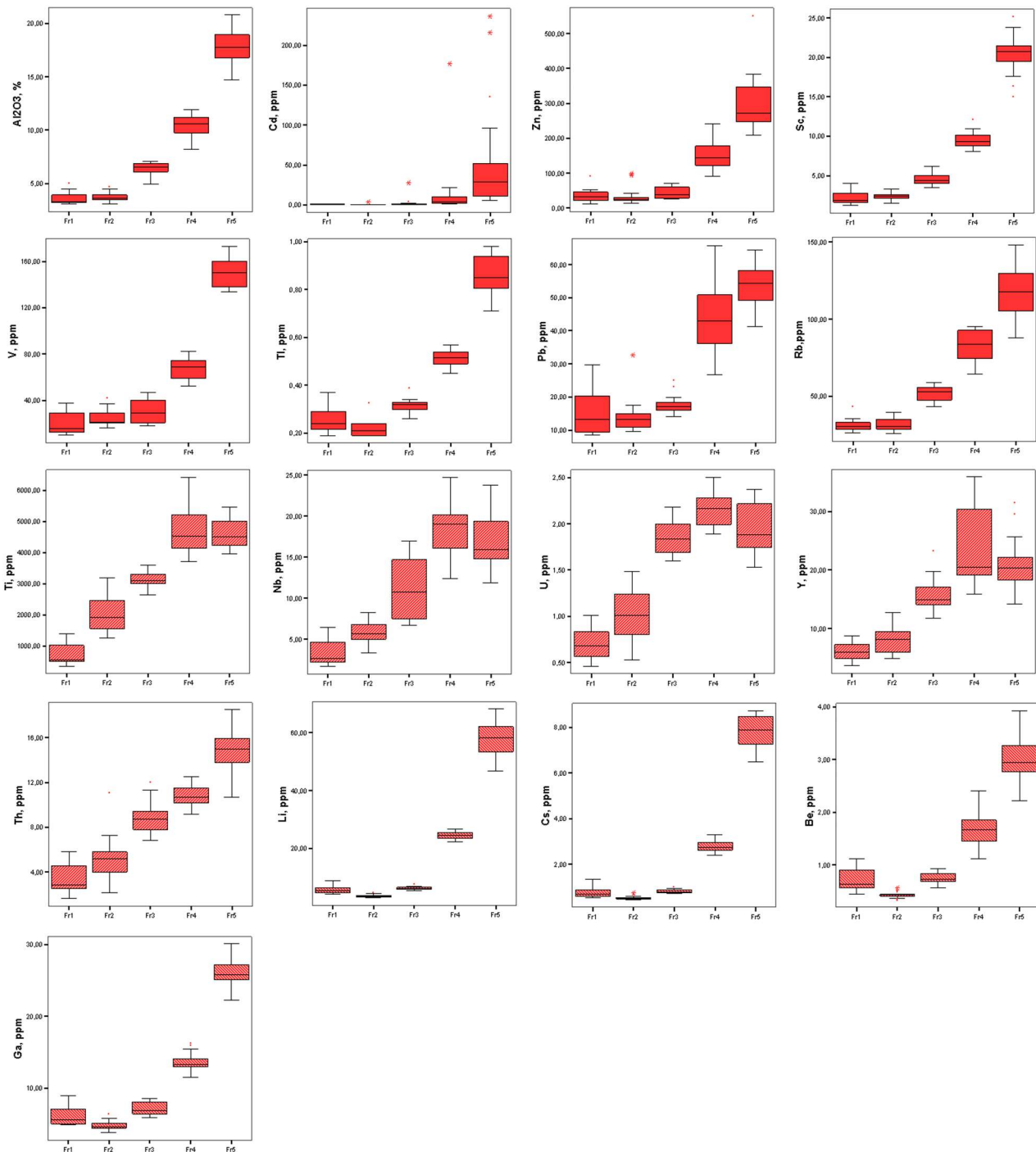
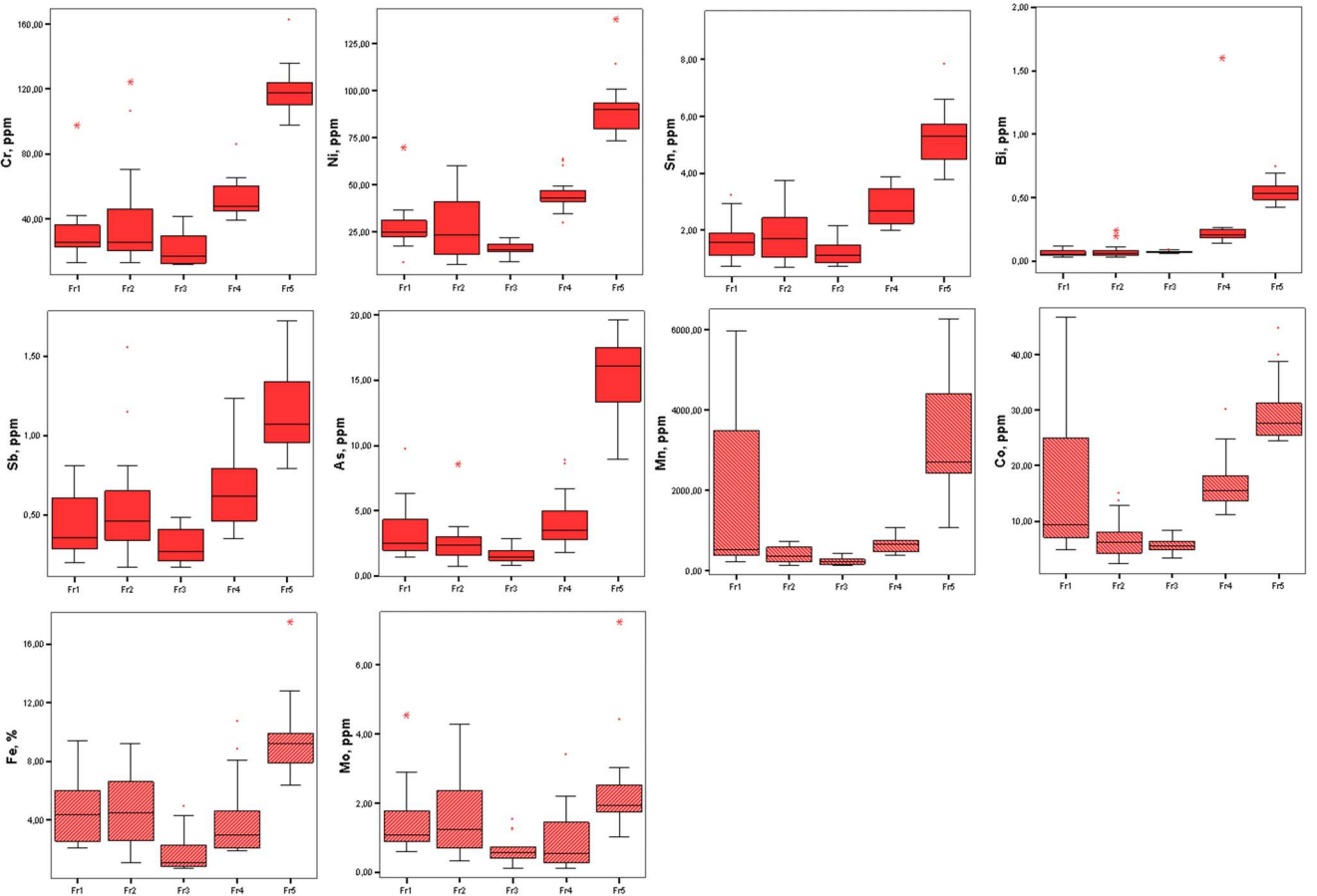


Figure S2. The abundances of elements (group A) in the soil particle size fractions. Median is indicated as a line across the box. X-axis: particle size fractions Fr1 – coarse and medium sand (250–1000 μm); Fr2 – fine sand (50–250 μm); Fr3 – coarse silt (10–50 μm); Fr4 – medium and fine silt (1–10 μm); Fr5 – clay (<1 μm).

101
102



103
104
105
106
107
108
109

Figure S3. The abundances of elements (group B) in the soil particle size fractions. Median is indicated as a line across the box. X-axis: particle size fractions Fr1 – coarse and medium sand (250–1000 µm); Fr2 – fine sand (50–250 µm); Fr3 – coarse silt (10–50 µm); Fr4 – medium and fine silt (1–10 µm); Fr5 – clay (<1 µm).

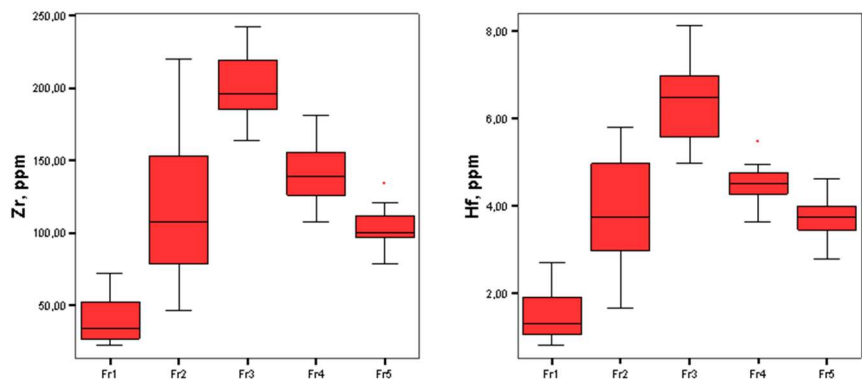


Figure S4. The abundances of elements (group C) in the soil particle size fractions. Median is indicated as a line across the box. X-axis: particle size fractions Fr1 – coarse and medium sand (250–1000 μm); Fr2 – fine sand (50–250 μm); Fr3 – coarse silt (10–50 μm); Fr4 – medium and fine silt (1–10 μm); Fr5 – clay (<1 μm).